J. Fluid Mech. (1990), *vol.* 220, *pp.* 485–514
Printed in Great Britain

Turbulence modulation in homogeneous dilute particle-laden flows

By R. N. PARTHASARATHY† AND G. M. FAETH‡
Department of Aerospace Engineering, The University of Michigan, Ann Arbor, MI 48109-2140, USA

(Received 25 August 1989)

Continuous-phase properties were studied for homogeneous dilute particle-laden flows caused by nearly monodisperse glass particles falling in a stagnant water bath. Test conditions included 0.5, 1.0 and 2.0 mm diameter particles (yielding particle Reynolds numbers based on terminal velocities of 38, 156 and 545) with particle volume fractions less than 0.01%. Measurements included mean and fluctuating velocities, as well as temporal spectra and spatial correlations of velocity fluctuations in the streamwise and cross-stream directions, using a two-point phase-discriminating laser velocimeter. Flow properties were also analysed using a stochastic method involving linear superposition of randomly-arriving particle velocity fields.

For present test conditions, liquid velocity fluctuations varied solely as a function of the rate of dissipation of particle energy in the liquid. The flows were highly anisotropic with streamwise velocity fluctuations being roughly twice cross-stream velocity fluctuations. Correlation coefficients and temporal spectra were independent of both particle size and the rate of dissipation of particle energy in the liquid. The temporal spectra indicated a large range of frequencies even though particle Reynolds numbers were relatively low, since both mean and fluctuating velocities in the particle wakes contributed to the spectra because particle arrivals were random. The theory predicted many of the features of the flows reasonably well but additional information concerning the mean and turbulent structure of the wakes of freely moving particles having moderate Reynolds numbers in turbulent environments is needed to address deficiencies in predictions of integral scales and streamwise spatial correlations.

1. Introduction

The objective of this investigation was to study turbulence modulation in dispersed multiphase flows, i.e. the direct modification of continuous-phase turbulence properties by transport from the dispersed phase (Al Taweel & Landau 1977). Turbulence modulation is most important in dense sprays and particle-laden flows, however, it is difficult to study in these circumstances owing to the complexities of the flows and limitations of instrumentation. To circumvent these problems a much simpler flow was considered; namely, a homogeneous dilute particle-laden flow generated by a uniform flux of particles moving through a nearly stagnant (in the mean) liquid so that all turbulence properties were due to the relative motion of the particles, i.e. the entire flow field was the result of turbulence modulation phenomenon.

† Present address: Institute of Hydraulic Research, University of Iowa, Iowa City, IO, USA.
‡ Author to whom correspondence should be addressed.

Past studies of turbulence modulation have been reviewed by Owen (1964, 1969), Hinze (1972) and Faeth (1987), while recent work can be found in Michaelides & Stock (1989). Hinze (1972) describes several mechanisms of turbulence modulation, as follows: (i) an effect due to locally increased shear rates in the continuous phase, modifying the turbulent energy spectrum of the continuous phase in the wavenumber range corresponding to the distance between elements of the dispersed phase; (ii) effects due to turbulence in the wakes of individual elements of the dispersed phase, modifying the turbulent energy spectrum of the continuous phase in the wavenumber range corresponding to the size of dispersed-elements; (iii) the action of groups of particles on the flow pattern of the continuous phase; and (iv) effects due to the volume occupied by the dispersed phase. Owing to the difficulties of making measurements in flows having large particle volume fractions, however, the last mechanism is not considered here, e.g. present particle volume fractions were less than 0.01 %. The remaining effects should influence the turbulence energy spectrum in wavenumber ranges corresponding to the size and spacing of the dispersed-phase elements which generally corresponds to the high-wavenumber range for most practical dispersed flows. According to Hinze (1972) modification of the turbulent energy spectrum at high wavenumbers implies greater dissipation rates than a single-phase flow having comparable mean-flow properties. This behaviour is supported by theoretical studies of particle motion in turbulent or turbulent-like flows with small relative velocities at the Stokes limit due to Kuchanov & Levich (1967), Owen (1969) and Al Taweel & Landau (1977).

In contrast, measurements suggest that effects of turbulence modulation are system-dependent and can cause turbulence levels to either increase or decrease. For example, studies reporting reduced turbulence levels attributed to turbulence modulation include: Owen (1969) who found reduced turbulence intensities in particle-laden pipe flows; Shuen *et al.* (1985) who found decreasing turbulence intensities with increasing particle loading in particle-laden turbulent jets; and Solomon *et al.* (1985) who found reduced turbulence levels and greater degrees of anisotropy in the dense region of sprays. On the other hand, studies reporting increased turbulence levels attributed to turbulence modulation include: Kada & Hanratty (1960) and Hino (1963) who found increased turbulence levels in pipe flows of suspensions; Sun & Faeth (1986) and Parthasarathy & Faeth (1987) who found increased turbulence and anisotropy levels in turbulent bubbly and particle-laden jets; and Lance & Bataille (1982) and Lance *et al.* (1980, 1985) who found increased turbulence levels in bubbly grid-generated turbulent flows and bubbly shear flows. Several phenomena are responsible for these differences in shear flows: the presence of the dispersed phase generally modifies mean velocity distributions to some extent, which influences conventional turbulence mechanisms that tend to dominate dispersed multiphase flows that are sufficiently dilute to be amenable to measurements; effects of turbulence modulation are influenced by both particle and turbulence properties which can lead to diverse behaviour even for similar flow configurations; and increased dissipation due to the presence of particles is counteracted by disturbances due to growing particle wakes which supplements turbulence generation by conventional single-phase mechanisms, particularly when the relative velocities of the particles are large.

Problems of interpreting effects of turbulence modulation are minimized in homogeneous flows like those considered by Lance & Bataille (1982) and Lance *et al.* (1985). Two air/water bubbly flow configurations were considered: nearly homogeneous flows downstream of a turbulence-generating grid and shear flows. In

general, continuous-phase turbulence intensities increased with increasing void fractions, with the largest increases observed at low liquid velocities where relative velocities were comparable to liquid velocities. This suggests that increased turbulence production due to the presence of bubble wakes dominated increased dissipation by the bubbles over the range of these experiments. The one-dimensional temporal spectra of streamwise velocity fluctuations were also modified by the presence of bubbles; in particular, the classical $-\frac{5}{3}$ power law for the inertial region of single-phase homogeneous turbulence was modified to a $-\frac{8}{3}$ power when bubbles were present, although temporal spectra were relatively independent of void fractions for the range of these tests. Lance *et al.* (1985) also achieved some success in modifying a second-order turbulence model to treat effects of turbulence modulation on the streamwise variations of the Reynolds stress tensor for the bubbly shear flow, however, these results were not evaluated for the homogeneous bubbly flows. Additionally, effects of turbulent dispersion could not be considered since bubble properties were not measured.

The present study seeks to extend the work of Lance & Bataille (1982) and Lance *et al.* (1985) by considering a homogeneous multiphase flow so that effects of turbulence modulation are highlighted. Rather than contend with the complications of grid-generated turbulence in a flowing continuous phase, however, the present study was limited to a uniform flux of nearly monodisperse spherical glass particles settling in a nearly stagnant (in the mean) water bath. This yields a stationary homogeneous flow where all turbulence properties are due to effects of turbulence modulation. Measurements included particle number fluxes, using Mie scattering from a laser light sheet; and liquid and particle velocities, and liquid temporal spectra and spatial correlations, using a two-point, phase-discriminating laser velocimeter. Stochastic analysis was also undertaken to assist interpretation of the measurements. The present paper is limited to effects of turbulence modulation: results relating to turbulent dispersion are reported in a companion paper (Parthasarathy & Faeth 1990).

Experimental and theoretical methods are described in the next two sections. Measured and predicted results are then presented in §4, considering evaluation of the apparatus, velocity fluctuations, temporal correlations and spatial correlations in turn. Major conclusions of the study are summarized in §5. Additional details and a complete tabulation of data can be found in Parthasarathy (1989).

2. Experimental methods

2.1. *Apparatus*

Figure 1 is a sketch of the homogeneous particle flow apparatus. The tests were conducted using nearly monodisperse spherical glass particles having nominal diameters of 0.5, 1.0 and 2.0 mm. The flow of particles was controlled by a variable-speed particle feeder (AccuRate, Model 310, having a 25 mm diameter helix for 0.5 mm diameter particles and a 19 mm diameter helix for 1.0 and 2.0 mm diameter particles, with centre rods used in both cases). The particles were dispersed by falling through an array of 9 screens (0.58 mm diameter wire spaced 2.1 mm apart for 0.5 and 1.0 mm diameter particles, and 0.89 mm diameter wire spaced 4.2 mm apart for 2.0 mm diameter particles) with a 190 mm spacing between screens. The particles then fell into a windowed tank ($410 \times 535 \times 910$ mm) which was filled with water to a depth of 800 mm. After a deceleration distance of 100–200 mm, the particles reached a steady (in the mean) terminal velocity within the bath. Measurements were

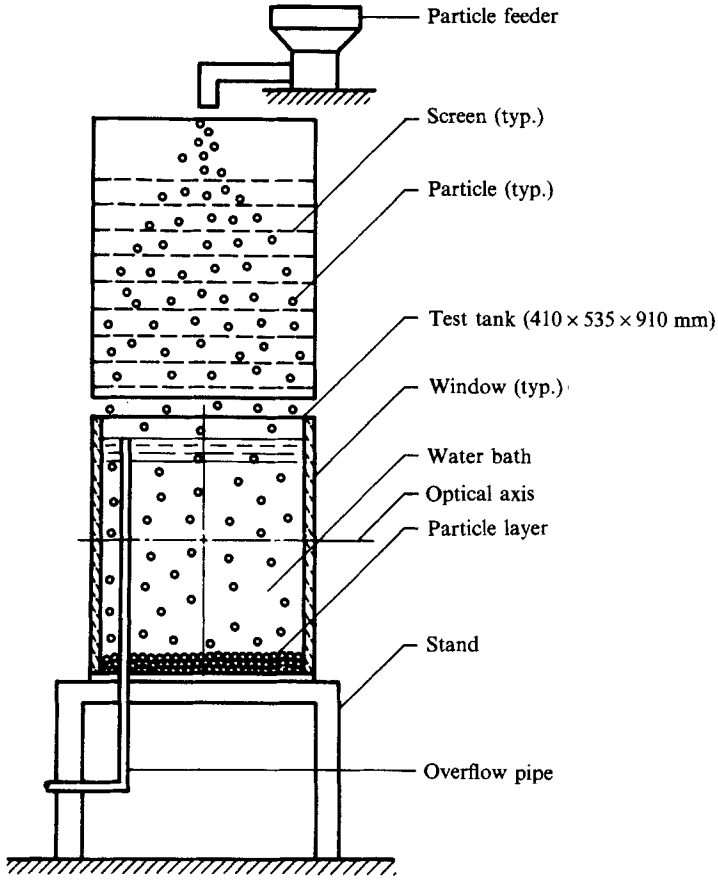

FIGURE 1. Sketch of homogeneous particle flow apparatus.

made near the centre of the tank, roughly at a depth of 400 mm. The particles collected at the bottom of the tank with little rebound upon impact and were removed from time-to-time using a suction system: the maximum depth of collected particles at the bottom of the tank was 100 mm. After collection, the particles were dried and reused since periodic examination showed negligible damage of used particles. Displacement velocities due to collection of particles at the bottom of the tank were less than 0.014 mm/s, which was negligible in comparison to the velocities of interest.

2.2. *Instrumentation*

Particle number fluxes were measured using a Mie scattering system similar to Sun & Faeth (1986). A small light sheet having a nearly uniform intensity was produced at the measuring volume by passing the beam from a 5 mW HeNe laser through an aperture. The measuring volume was observed in a horizontal plane, normal to the laser beam, using a photodetector. Particles passing through the measuring volume generated pulses in the detector output which were shaped and recorded by a pulse counter developed in this laboratory. The pulse counter had an adjustable threshold to control spurious background signals. Grazing collisions of particles with the optical measuring volume were recorded so that the region observed had dimensions that were roughly the sum of optical lengths and the particle diameter. The actual

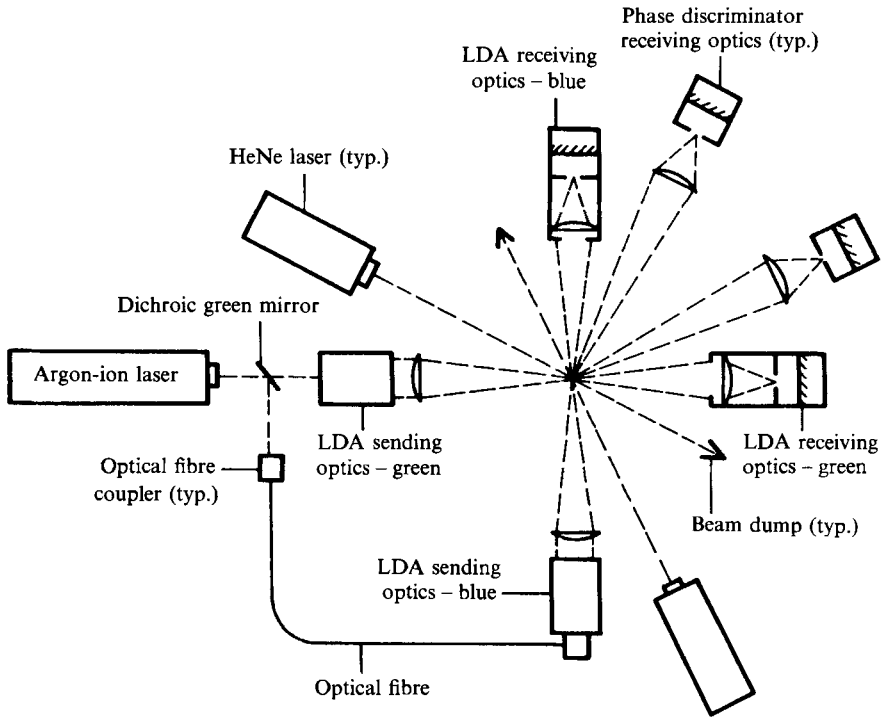

FIGURE 2. Sketch of two-point phase-discriminating laser velocimeter.

area of observation, however, was calibrated by collecting particles for timed intervals. More than 500 particles were counted to find the mean particle number flux. Experimental uncertainties were due to variations of particle diameters within each size group, which influenced the area observed, and finite sampling times: the latter dominated the measurements yielding experimental uncertainties (95% confidence) less than 10% (Parthasarathy 1989).

A two-point, phase-discriminating laser velocimeter (LV) was used to measure mean and fluctuating velocities, and one- and two-point correlations of velocity fluctuations of the liquid; as well as streamwise and cross-stream particle velocities. Figure 2 is a schematic diagram of the LV arrangement. The LV involved one fixed channel, focused at the centre of the tank, and one channel that could be traversed in both the streamwise and cross-stream directions. The two channels were based on the green (514.5 nm) and blue (488 nm) lines of a 2W argon-ion laser operating in the multiline mode. The two laser lines were separated with a dichroic green mirror and the blue line was transmitted to the sending optics of the traversable channel using a fibre-optic cable. Both channels operated in the dual-beam forward-scatter mode and had measuring volumes with diameters of 0.1 mm and lengths of 1.2 mm. Directional bias and ambiguity were eliminated using a 40 MHz Bragg-cell frequency shifter (TSI, Model 918-11) with the output signals downshifted to convenient frequency ranges (0.05–0.1 MHz) for filtering and signal processing. Streamwise and cross-stream velocities were measured by rotating the LV optics accordingly.

One-half gram of titanium dioxide particles in rutile form (nominal diameter of 2.8 μm) were used to seed the bath for the LV measurements. It took about 15 minutes to distribute the seeding particles throughout the bath and 12 hours for them to settle to the bottom. Since the longest test time was roughly 3 hours, settling

of seeding particles did not alter data rate appreciably. This seeding level provided data rates of 2–4 kHz over the test range.

Light scattered by the seeding particles generally yielded lower amplitude signals than light scattered by the glass beads so that simple amplitude discrimination could be used to detect particle velocity signals. As Modarress, Tan & Elghobashi (1984) point out, however, particles grazing the LV measuring volume can yield low-amplitude signals which could be misinterpreted as liquid-phase velocity signals: this is a serious problem for the present experiments since relative velocities between the phases were large in comparison to liquid velocities. Thus a phase-discriminating system, illustrated in figure 2, was used on both channels to avoid biasing of liquid velocities due to grazing collisions. The arrangement involved a third beam from a 5 mW HeNe laser at an angle of 18° from the LV axis which was observed off-axis in the forward-scatter direction at an angle of 32° from the LV axis. This yielded a discriminator measuring volume having a diameter of 0.6 mm and a length of 1.3 mm which enveloped the LV measuring volume. Thus, particles that grazed the measuring volume yielded a scattering signal that was detected by the discriminator system. The data processing system was programmed to eliminate all liquid-phase velocity records where the discriminator signal indicated the presence of a particle near the LV measuring volume. For present conditions, however, the effects of grazing collisions were small since the flows were dilute, e.g. operation with and without the phase discriminators resulted in less than 2% changes of velocity fluctuations.

The time between valid liquid velocity signals was small, *c.* 0.5–1 ms, in comparison to Kolmogorov timescales in the range 66–177 ms and integral timescales in the range 4–7 s; therefore, the analogue outputs of the burst-counter signal processors (TSI Model 1980B) were time-averaged, ignoring periods when particles were present, to obtain unbiased time-averaged liquid velocities. The analogue outputs were filtered using Ithaco low-pass filters before the signals were digitized and transferred to a microcomputer for processing. It was found that averaging signals for twenty minutes provided satisfactory values of mean and fluctuating velocities, probability density functions and two-point velocity correlations. One-point temporal spectra were measured over a frequency range of 10^{-4}–10^{3} Hz. These spectra were obtained using three sampling frequencies: 7.5, 50 and 2500 Hz with low-pass filter settings of 4, 25 and 1000 Hz. The spectra were obtained from 4096 points at each sampling frequency, averaging over 80–90 such groups to obtain final results. The spectra at different sampling frequencies overlapped and were matched at the common frequencies before normalizing the total area under the combined spectrum to unity.

Bias errors were small since the flow was homogeneous. Experimental uncertainties (95% confidence) were dominated by finite sampling times and were as follows: mean streamwise and cross-stream velocities, less than 10% and 40%; fluctuating streamwise and cross-stream velocities, less than 14% and 21%; temporal spectra of streamwise and cross-stream velocity fluctuations, less than 35% and 42% for frequencies below 0.01 Hz and less than 16% and 21% for all other frequencies; two-point spatial correlations in the lateral and streamwise directions, less than 29% and 36%; and Reynolds stresses less than 55% (Parthasarathy 1989). These values are high in comparison to typical turbulent flows due to very low liquid velocities (*c.* 10 mm/s) and very high turbulence intensities (in excess of 100%).

Particle diameter (mm)	0.5 (0.045)		1.0 (0.085)		2.0 (0.15)	
Particle loading	Low	High	Low	High	Low	High
Particle properties:						
Terminal velocity (mm/s)	65 (7)		147 (14)		262 (16)	
Reynolds number (−)	38 (9)		156 (20)		545 (53)	
Drag coefficient (−)	2.08		0.90		0.61	
Number flux (kpart/m^2 s)	55.4	110.8	3.7	20.9	1.1	3.3
Mean spacing (mm)	10.5	8.2	32.7	18.3	61.8	43.2
Liquid properties:						
Rate of dissipation (mm^2/s^3)	53.2	106.3	27.3	155.8	61.7	193.5
l_K (mm)	0.33	0.28	0.39	0.25	0.32	0.24
t_K (s)	0.13	0.09	0.18	0.07	0.12	0.07
u_K (mm/s)	2.6	3.1	2.2	3.4	2.7	3.6
$(\overline{u'^2})^{\frac{1}{2}}$ (mm/s)	3.3	4.7	2.4	5.1	3.7	6.1
$(\overline{v'^2})^{\frac{1}{2}}$ (mm/s)	1.6	2.7	1.2	2.3	1.7	3.1
$\bar{u}$ (mm/s)	1.6	3.9	1.0	3.8	3.0	6.0
$\bar{v}$ (mm/s)	0.7	0.6	1.1	1.6	1.0	0.9

TABLE 1. Representative test conditions. Round glass beads, density of 2450 kg/m^3, falling in a stagnant water bath at 298 ± 2 K. Numbers in parentheses denote standard deviations. Particle volume fractions less than 0.01 %, displacement velocities less than 0.014 mm/s, direct, dissipation by particles less than 4.5 %.

2.3. *Test conditions*

A range of particle number fluxes were considered for each particle size; representative test conditions at the low and high ends of these ranges are summarized in table 1. Measured particle size distributions were approximately Gaussian and had standard deviations of roughly 10% of the nominal particle diameter. Particle drag properties were calibrated by releasing individual particles within the still water bath and measuring their terminal velocities with the LV system. The measured probability density functions (PDFs) of terminal velocities were then compared with predicted PDFs based on the measured size distribution and the standard drag coefficient, C_D, for spheres (Putnam 1961):

$$C_D = 24(1 + \tfrac{1}{6}Re^{\frac{2}{3}})/Re, \tag{1}$$

where the particle Reynolds number is defined as

$$Re = U_\infty d_p/\nu, \tag{2}$$

and U_∞ is the terminal velocity, d_p the particle diameter and ν the kinematic viscosity of water. Particle Reynolds numbers were 38, 156 and 545 for the 0.5, 1.0 and 2.0 mm diameter particles. Matching predicted and measured mean terminal velocities required corrections to the standard drag coefficient of less than 14 %: the resulting corrected drag coefficients and terminal velocities for each particle size appear in table 1. The terminal velocities of particles passing through the dispersing screen, both singly and at test particle fluxes, were not appreciably different from the calibrated terminal velocities.

Mean particle spacings, l_p, were found assuming that particles were falling randomly with a uniform particle number flux $\dot{n}''$, and a mean particle-averaged terminal velocity, $\tilde{u}_p$:

$$l_p = (\tilde{u}_p/\dot{n}'')^{\frac{1}{3}}. \tag{3}$$

The resulting particle spacings were in the range 8–62 mm, or 16–33 particle

diameters, yielding particle volume fractions less than 0.01%; therefore, effects of direct particle-to-particle interactions were small.

Within the region where measurements were made, the mean velocities of the particles were constant and were much greater (*c.* 10 times greater) than their velocity fluctuations. Additionally, the particles showed no evidence of rotation as they entered the bath or during their descent in the bath. Then the rate of dissipation of turbulence kinetic energy, ϵ, within the bath can be equated to the rate of production of turbulence by particles assuming that effects of particle velocity fluctuations are small. The rate of production of turbulence is then equal to the rate of loss of the potential energy of the particles as they fall through the bath, yielding

$$\epsilon = \pi \dot{n}'' g d_p^3 \tfrac{1}{6}(\rho_p - \rho)/\rho, \tag{4}$$

where g is the acceleration due to gravity and ρ_p and ρ are the particle and bath densities. Dissipation was used to characterize the measurements since it provides a basis for comparing results for different particle sizes and number fluxes using a single parameter; thus, representative values of ϵ appear in table 1. The corresponding Kolmogorov length, $l_K = (\nu^3/\epsilon)^{\frac{1}{4}}$, time, $t_K = (\nu/\epsilon)^{\frac{1}{2}}$ and velocity $u_K = (\epsilon\nu)^{\frac{1}{4}}$ scales also appear in the table. Notably, the Kolmogorov lengthscale is comparable to the LV measuring volume and somewhat smaller than the particle diameters. Furthermore, measured liquid streamwise and cross-stream velocity fluctuations, $(\overline{u}'^2)^{\frac{1}{2}}$ and $(\overline{v}'^2)^{\frac{1}{2}}$, are comparable to the Kolmogorov velocity scales although the u_K varies to a lesser extent as ϵ is changed. The effect of mean streamwise and cross-stream velocities, $\overline{u}$ and $\overline{v}$, in the flows, summarized in table 1, will be taken up later.

In a particle-laden flow, the dissipation of turbulence consists of two components: conventional dissipation by the continuous phase; and direct dissipation by interactions between the particles and the continuous phase – the last being the contribution that was ignored when deriving (4) as well as the contribution that is usually considered in turbulence models of the process (Faeth 1987). The relative importance of these two contributions to dissipation can be found by noting that the instantaneous rate of dissipation per particle, ϵ_p, is equal to the product of the drag force and the relative velocity:

$$\epsilon_p = 3\pi\nu d_p(1 + \tfrac{1}{6}Re^{\frac{2}{3}})\, u_r^2, \tag{5}$$

where the drag coefficient has been obtained from (1) and u_r is the relative velocity. The time-averaged dissipation per particle is then given by

$$\overline{\epsilon}_p = 3\pi\nu d_p[(1 + \tfrac{1}{6}Re^{\frac{2}{3}})\, \overline{u}_r^2 + (1 + 10Re^{\frac{2}{3}}/27)\, \overline{u}_r'^2], \tag{6}$$

where $\overline{u}_r$ and $\overline{u}_r'^2$ are the mean value and variance of the relative velocity. The first term on the right-hand side of (6) is dissipation due to the mean drag and relative velocity: it is the component of dissipation per particle that is analogous to the production of turbulence considered in (4). The second term on the right-hand side of (6) represents the direct contribution of the particle to the dissipation of turbulence: it is the product of the fluctuating drag force and the fluctuating relative velocity. Parthasarathy (1989) estimates upper bounds for the ratio of the two terms, finding that the second term is generally less than 5% of the first term for present test conditions since $\overline{u}_r'^2/\overline{u}_r^2$ is small. Thus, generation of turbulence by particles, followed by dissipation within the liquid, are the dominant features for present test conditions, while direct dissipation of turbulence by particles is a secondary effect. Furthermore, ignoring the second term when estimating ϵ from (4) is reasonably accurate for present conditions as well.

3. Theoretical methods

3.1. *General formulation*

Simplified analysis of the flow was undertaken in order to help interpret measurements of liquid-phase properties. Two limiting analyses of the liquid phase were considered: (i) methods used to treat homogeneous turbulent flows with time-averaged governing equations for turbulence quantities, analogous to those considered by Hinze (1975) for isotropic turbulence; and (ii) methods that explicitly consider the properties of the flow field of individual particles, analogous to the approach of Batchelor (1972) for sedimentation processes. Methods used for isotropic turbulence have been applied to grid-generated turbulence where the grid plays a role similar to the particles in the present flows; however, these methods are only applied at some distance from a grid of close-spaced elements where the properties of the near field behind the grid have been lost, yielding a non-stationary decaying isotropic flow. This is not very appealing for the present problem where the flow is stationary and wake sources are present throughout the flow field, i.e. the particles are widely spaced in comparison to their dimensions so that strong interactions between neighbouring wakes do not immediately occur and wakes remain identifiable for some distance before losing their character through interactions with other nearby wakes. Thus, a method that explicitly considers the flow field of the particles, similar to Batchelor (1972), was pursued instead.

The major assumptions of the analysis are: the flow is statistically stationary with a uniform flux of particles and constant liquid properties; particle arrival times at an increment of area are independent of other particle arrival times so that arrival times satisfy Poisson statistics (Rice 1954); the flow was taken to be infinite in extent since the measurements exhibited little effect of bath volume; and the flows are dilute so that the probability of a test point being within a particle is negligibly small. The flow field associated with each particle included the following contributions: the near-field flow around the particle, which was taken to be the potential flow around a sphere since the probability of a point of observation being in the strongly viscous region near the surface is small in dilute flows; and the asymptotic properties of the particle wake. The equations of motion are linear for potential flow and for asymptotic wake flow; therefore, we can assume that flow properties are the result of a linear superposition of the particle flow fields that have reached the point of observation.

Summing flow properties under these assumptions involves extension of methods used to analyse random noise when effects of noise can be added linearly (Rice 1954). Let the point of observation be the origin of a cylindrical coordinate system with x denoting the streamwise direction and r and ϕ denoting the radial and azimuthal coordinates. Since wake Reynolds numbers exceed unity for present conditions, effects of wake turbulence can be important (Tennekes & Lumley 1972); therefore, we suppose that arrival of a particle at $x = 0, r, \phi$ and time $t = 0$ produces effects $g(r, \phi, t)$ due to mean properties and $g'(r, \phi, t)$ due to turbulent properties at the point of observation. Then, if the effect of each particle can be added linearly, the total effect due to all particles at time t is:

$$G(t) = \sum_{j=0}^{\infty} \sum_{k=-\infty}^{\infty} (g(r_j, \phi_j, t-t_{jk}) + g'(r_j, \phi_j, t-t_{jk})), \tag{7}$$

where the position vectors (r_j, ϕ_j) are chosen to collect all particles, and the kth particle at position (r_j, ϕ_j) reaches $x = 0$ at t_{jk}.

Following Rice (1954), Campbell's theorem can be extended to treat random arrivals of particles over a plane to yield the time-averaged effect:

$$\bar{G} = \dot{n}'' \int_{-\infty}^{\infty} \mathrm{d}t \int_{0}^{2\pi} \mathrm{d}\phi \int_{0}^{\infty} g(r, \phi, t)\, r\, \mathrm{d}r, \tag{8}$$

while the mean-squared fluctuation about the average becomes:

$$\bar{G'^2} = \dot{n}'' \int_{-\infty}^{\infty} \mathrm{d}t \int_{0}^{2\pi} \mathrm{d}\phi \int_{0}^{\infty} (g^2(r, \phi, t) + g'^2(r, \phi, t))\, r\, \mathrm{d}r. \tag{9}$$

Rice (1954) also shows that the probability-density function (p.d.f.) of G approaches a normal distribution as $\dot{n}'' \to \infty$. For finite $\dot{n}''$, the error in approximating the p.d.f. by the normal distribution is on the order of $\bar{G'^3}/(\bar{G'^2})^2 \sim 1/\dot{n}''$, which is small for present test conditions.

Temporal correlations and spectra, and spatial correlations, are also of interest since they affect the turbulent dispersion of the particles. Proceeding as before (Rice 1954), the temporal correlation of G with time delay τ, is given by

$$\overline{G'(t)\, G'(t+\tau)} = \dot{n}'' \int_{-\infty}^{\infty} \mathrm{d}t \int_{0}^{\infty} (g(r, \phi, t)\, g(r, \phi, t+\tau) + g'(r, \phi, t)\, g'(r, \phi, t+\tau))\, r\, \mathrm{d}r. \tag{10}$$

The temporal spectrum is obtained from the Fourier transform of (10):

$$E_G(f) = 4 \int_{0}^{\infty} \overline{G'(t)\, G'(t+\tau)} \cos(2\pi f \tau)\, \mathrm{d}\tau, \tag{11}$$

where f denotes frequency. The spatial correlation in the cross-stream direction is most conveniently found in a Cartesian coordinate system with Y and Z denoting coordinates in a cross-stream plane and y the separation distance between points, with no loss of generality since the flow is homogeneous. Then, the spatial correlation of G' in the cross-stream direction is

$$\overline{G'(Y)\, G'(Y+y)} = \dot{n}'' \int_{-\infty}^{\infty} \mathrm{d}t \int_{-\infty}^{\infty} \mathrm{d}Z \int_{-\infty}^{\infty} [g(Y, Z, t)\, g(Y+y, Z, t) + g'(Y, Z, t)\, g'(Y+y, Z, t)]\, \mathrm{d}Y. \tag{12}$$

In order to find the spatial correlation of G' in the streamwise direction we assume that the particles are moving in the x-direction at their terminal velocities, since particle velocity fluctuations are small in comparison to U_∞. This implies that effects of turbulent particle dispersion are small, which is only appropriate at the limit of infinitely dilute flow. Thus, the spatial correlation at displacement x is the same as the temporal correlation at delay time τ with $x = U_\infty \tau$, or

$$\overline{G'(X)\, G'(X+x)} = \overline{G'(U_\infty t)\, G'(U_\infty (t+\tau))}. \tag{13}$$

Several properties of the flow can be inferred immediately from (9)–(13) before specifying wake properties and completing the integrations. In particular, since $\epsilon \sim \dot{n}''$ from (4), effects of dissipation can be summarized as follows for a particular particle size: velocity fluctuations are proportional to $\epsilon^{\frac{1}{3}}$; correlations and temporal spectra are proportional to ϵ; and correlation coefficients, normalized temporal

spectra, ratios of velocity fluctuations, and temporal and spatial integral scales are all independent of ϵ.

The preceding equations are limited to monodisperse particle flows. However, under the assumption of linear superposition, if $\phi(d_p)$ is a generic property for a particular particle diameter, then the mean value of ϕ becomes:

$$\bar{\phi} = \int_0^\infty \phi(d_p)\,\text{p.d.f.}\,(d_p)\,\mathrm{d}d_p, \tag{14}$$

where the p.d.f. (d_p) was measured as noted earlier.

3.2. *Particle flow field and liquid properties*

The properties to be found from (8)–(13) can be separated into three components that can be valuated separately and summed. For a generic property ϕ, this includes the potential flow region, ϕ_{pf}; the mean properties of the wake, ϕ_{mw}; and the turbulent properties of the wake, ϕ_{tw}. Potential flow properties were found by assuming that effects of velocity fluctuations in the flow experienced by the particle could be ignored. This is reasonable since the relative turbulence intensities of the particles, which are comparable to $(\overline{u'^2})^{\frac{1}{2}}/U_\infty$, are small even though particle diameters are somewhat larger than the Kolmogorov lengthscales. For a sphere moving in a stagnant fluid the potential flow velocities are (Batchelor 1973):

$$u = (\tfrac{1}{16}U_\infty d_p^3/r_0^3)\,(1+x^2/r_0^2), \tag{15}$$

$$v = (\tfrac{1}{16}U_\infty d_p^3\,x/r_0^4)\,(1-x^2/r_0^2)^{\frac{1}{2}}, \tag{16}$$

where the centre of the sphere is the instantaneous origin, r_0 is the distance from the point of observation to the centre of the sphere, and x is the streamwise distance from the centre of the sphere. To convert (15) and (16) to a coordinate system fixed at the point of observation, we use the following transformations:

$$x = U_\infty t, \quad r_0^2 = U_\infty^2 t^2 + r^2. \tag{17}$$

The velocities of (15) and (16) decay rapidly with distance from the sphere and are practically zero at $r_0 = 2d_p$; therefore, potential flow calculations were terminated at $r = 2d_p$ and wake properties were used beyond this point. Mean-squared velocity fluctuations for the potential flow region then become:

$$\overline{u'^2_{pf}} = 0.019\epsilon d_p^3/(U_\infty \theta^2), \tag{18}$$

$$\overline{v'^2_{pf}} = 0.003\epsilon d_p^3/(U_\infty \theta^2), \tag{19}$$

where

$$\theta = (\tfrac{1}{8}C_D\,d_p^2)^{\frac{1}{2}}. \tag{20}$$

The contributions of the potential flow region to velocity fluctuations from (18) and (19) were less than 10% of the contributions of the wakes since the volume of the potential flow region is much smaller than the wake. Thus, the contributions of the potential core were only considered for $\overline{u'^2}$ and $\overline{v'^2}$ but were ignored for other properties.

Specifying a representative wake is complicated by turbulent dispersion of the freely moving particles and the turbulence of the flow field itself which modifies the structure of the particle wakes from properties found with rigidly-mounted spheres is non-turbulent environments. For lack of an alternative, however, we consider the

limit of an infinitely dilute flow where these disturbances are small and the particle and its wake follow a vertical path. The mean liquid downflow velocity due to particle motion is also negligible at this limit so that velocities outside the wake are negligible. The following discussion will be limited to turbulent wakes, Parthasarathy (1989) presents the formulation for laminar wakes. The mean velocity distributions in turbulent wakes were derived from results appearing in Tennekes & Lumley (1972):

$$\bar{u}/U_\infty = 2.23(U_\infty t/\theta)^{-\frac{2}{3}}\exp(-r^2/2l^2), \tag{21}$$

$$\bar{v}/U_\infty = 0.74\theta^{\frac{2}{3}}r(U_\infty t)^{-\frac{5}{3}}\exp(-r^2/2l^2), \tag{22}$$

where

$$l = 0.47(U_\infty t\theta^2)^{\frac{1}{3}}, \tag{23}$$

and (17) has been used to convert from distance from the sphere to time after arrival of the sphere. Finally, the local wake Reynolds number is

$$Re_l = (U_\infty\theta/\nu)(\theta/U_\infty t)^{\frac{1}{3}}. \tag{24}$$

From (24) it is evident that Re_l progressively decreases with increasing time, eventually reaching laminar wake conditions if the ambient environment is not turbulent. Equations (21)–(23) are based on similarity assumptions with a constant eddy viscosity over the wake cross-section at asymptotic conditions far from the sphere. In spite of these simplifications, however, (21) provides a reasonable correlation of the existing measurements of Uberoi & Freymuth (1970) for the wakes of rigidly-mounted spheres in a non-turbulent environment. The values of $\bar{u}$ and $\bar{v}$ from (21) and (22) are unbounded at small t but the equations are only used in the present wake region where $t > T_0 = 2d_p/U_\infty$.

Inserting (21)–(23) into (8)–(13) showed that except for $\bar{v}'^2_{mw}$, the integrals did not converge as $t \to \infty$. A similar problem is encountered for laminar wake properties so that eventual transition to a laminar wake does not resolve the difficulty. This problem is similar to limit problems encountered for Stokes flow around particles during analysis of sedimentation where resolving the problem benefited from a rigorous knowledge of Stokes flow (Batchelor 1972). In the present case, (21)–(23) are empirical and their relevance to the turbulent environment of the present flows certainly is questionable; therefore, rather pursue the limit problem the present results were found for a finite upper limit of integration, T_∞, assuming that at this point wake properties have lost coherence in the turbulent field. The value of T_∞ is specified later to fit measured and predicted velocity fluctuations. The general results are:

$$u'^2_{mw} = 3.34\epsilon(\theta^2 T_\infty/U_\infty^2)^{\frac{1}{3}}, \tag{25}$$

$$\bar{v}'^2_{mw} = 0.014\epsilon\theta^2(T_\infty - T_0)/(T_0\,T_\infty\,U_\infty^2), \tag{26}$$

$$\overline{u'(t)\,u'(t+\tau)_{mw}} = 2.23\epsilon(\theta/U_\infty)^{\frac{2}{3}}\int_{T_0}^{T_\infty}(t^{\frac{2}{3}} + (t+\tau)^{\frac{2}{3}})^{-1}\,dt, \tag{27}$$

$$\overline{v'(t)\,v'(t+\tau)_{mw}} = 0.056\epsilon(\theta/U_\infty)^2\int_{T_0}^{T_\infty}(t(t+\tau)^{-\frac{1}{3}})\,(t^{\frac{2}{3}} + (t+\tau)^{\frac{2}{3}})^{-2}\,dt, \tag{28}$$

$$\overline{u'(Y)\,u'(Y+y)_{mw}} = 1.11\epsilon(\theta/U_\infty)^2\int_{T_0}^{T_\infty}(t^{-\frac{2}{3}}\exp(1.11y^2(U_\infty t\theta^2)^{-\frac{2}{3}})\,dt, \tag{29}$$

where the integrals in (27)–(29) were found numerically after T_∞ was specified.

Turbulence intensities of wakes are large even near the axis so that the contribution of wake turbulence to (8)–(12) is significant. Wake turbulence properties used during the calculations were taken from Uberoi & Freymuth (1970) which involved wake Reynolds numbers in the range 4000–150 000. Present wake Reynolds numbers were much lower, with local values in the range 2–500 for the present final selection of T_∞, so that computed results can be thought of as an upper bound for effects of wake turbulence on various properties at the limit of low particle number fluxes. Based on numerical integration of the measurements of Uberoi & Freymuth (1970), we immediately get the following relationships between mean and fluctuating velocities in the wakes:

$$\overline{u}'^2_{\mathrm{tw}}/\overline{u}'^2_{\mathrm{mw}} = 1.50, \quad \overline{v}'^2_{\mathrm{tw}}/\overline{u}'^2_{\mathrm{mw}} = 1.15. \tag{30}$$

Uberoi & Freymuth (1970) found that spectra at various points in the wake were identical at low frequencies when normalized by integral scales, and at high frequencies when normalized by Kolmogorov scales. These spectra were integrated in terms of normalized variables and then matched at intermediate frequencies. This gives the following contribution of wake turbulence to the temporal spectra of streamwise velocity fluctuations

$$\begin{aligned} E_{u_{\mathrm{tw}}}/\overline{u}'^2_{\mathrm{tw}} &= 0.0036 \text{ Hz} \quad (0 < f < 230), \\ &= 1.04 \times 10^6 f^{-3.59} \quad (230 < f < 2000), \end{aligned} \tag{31}$$

where f is the frequency in Hz. The same form was used for the cross-stream temporal spectra, $E_{v_{\mathrm{tw}}}$, since the temporal spectra of cross-stream velocity fluctuations were virtually identical to streamwise velocity fluctuations (Uberoi & Freymuth 1970).

Measurements of lateral spatial correlations in turbulent wakes are not available; therefore, these correlations were calculated based only on mean wake properties. The turbulent contribution to the streamwise spatial correlation was obtained from the temporal correlation as discussed earlier.

4. Results and discussion

4.1. *Evaluation of apparatus*

Initial experiments dealt with evaluation of the apparatus, considering uniformity of particle number fluxes, homogeneity of liquid flow properties, effects of wave action at the liquid surface, effects of bath size, approach to steady state conditions, mean velocities and Reynolds stresses.

Measurements of particle number fluxes as a function of position are illustrated in figure 3. The 1.0 mm diameter particles are considered at low, medium and high loadings having dissipation rates of 27.3, 68.2 and 155.8 $\mathrm{mm}^2/\mathrm{s}^3$. The measurements only extend to the near-wall region on one side due to limitations of traversing the Mie-scattering measuring volume. The particle number fluxes are uniform within experimental uncertainties ($\pm 10\%$) over the middle 300 mm of the bath cross-section. Reduced particle number fluxes in the near-wall region are attributed to the fact that the duct for the particle feed system was 30 mm smaller (in each direction) than the liquid bath. Collection of particles at the bottom of the bath revealed that particle fluxes were uniform in the other direction as well, except within 50 mm of walls.

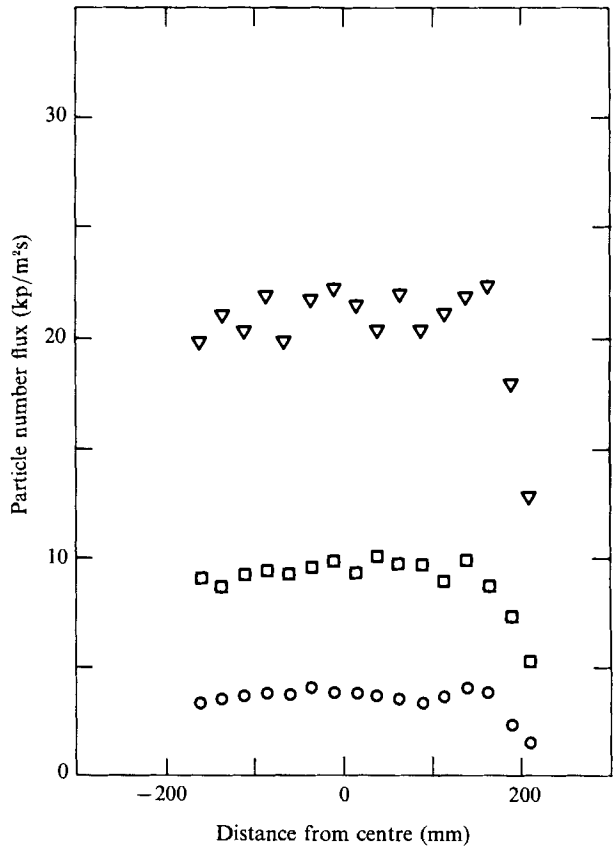

FIGURE 3. Particle number flux distribution for 1 mm diameter particles: ○, $\epsilon = 27.3$ mm^2/s^2; □, 68.2 mm^2/s^2; ▽, 155.8 mm^2/s^2.

The variation of streamwise liquid velocity fluctuations across the bath are illustrated in figure 4 for the same test conditions as figure 3. Open and shaded symbols represent measurements 100 mm above and below the location of the measuring volume of the fixed LV channel. Similar to the particle number fluxes, the streamwise velocity fluctuations are uniform within experimental uncertainties over the central 300 mm cross-section of the bath. In addition, velocity fluctuations measured at different points in the central region of the bath during the spatial correlation measurements for all three particle sizes also exhibited constant values within experimental uncertainties. Thus, we conclude that liquid properties were homogeneous within the region of measurements for all test conditions.

Effects of surface waves were examined by damping them with a honeycomb at the liquid surface (10 mm cell size, 50 mm thick) with the mean liquid level at the midpoint of the honeycomb. The particles passed through the honeycomb with no difficulty. Virtually no change in streamwise velocity fluctuations was detected with the honeycomb installed; therefore, it was removed for the remainder of the tests for operational convenience.

Disturbances of the uniformity of the particle number fluxes were studied by placing 50 mm wide strips, both one at a time and in pairs adjacent to opposite walls of the bath, with the centres of the strips 50–70 mm from the walls. The effects of these disturbances on streamwise velocity fluctuations at the centre of the bath was

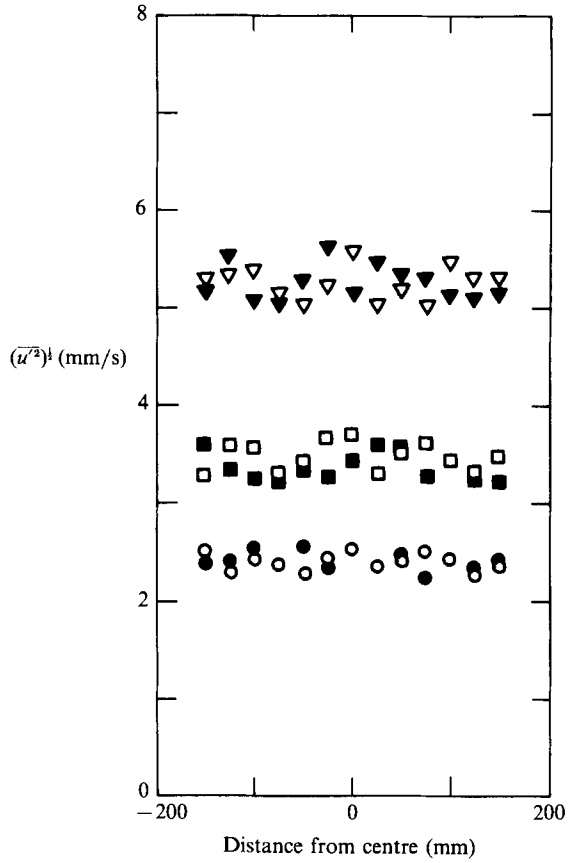

FIGURE 4. Streamwise liquid velocity fluctuation distributions for 1 mm diameter particles: ○, ●, $\epsilon = 27.3$ mm^2/s^3; □, ■, 68.2 mm^2/s^3; ▽, ▼, 155.8 mm^2/s^3. Open and filled symbols denote positions 100 mm above and below the measuring location, respectively.

generally less than 10%, except for a 15% change with two strips parallel to the 410 mm walls. Such massive uniformities are not likely in view of the measurements illustrated in figure 3; therefore, potential effects of particle flux non-uniformities were well within the experimental uncertainties of the velocity measurements.

Effects of the volume of the liquid bath were studied by placing two boxes constructed of Plexiglas (interior cross-sections of 200 × 200 mm and 100 × 100 mm and heights of 900 mm) within the bath along the centreline. Streamwise velocity fluctuations were then measured for full liquid heights, as well as half liquid height in the 100 × 100 mm box – the last bath volume being $\frac{1}{32}$ of the full bath volume. The smallest bath volume yielded streamwise velocity fluctuations that were only 10% lower than the full bath volume so that it is not likely that present results were influenced to a significant extent by the bath surfaces. This is reasonable since spatial integral scales in the cross-stream and streamwise directions were 15–21 mm and 57–59 mm, which are 5–7 times smaller than the corresponding dimensions in the smallest bath volume that was tested. Test results reported here were obtained in the full-size bath where these ratios are 2–4 times larger.

The approach of the liquid bath to stationary conditions and the capability of the particle feeder to maintain these conditions for test periods of hours were also studied. This was done by ensemble averaging measurements for several tests where

the particle feeder was started and operated for 75 minutes, considering the 100×100 mm and 200×200 mm baths as well as the full bath. It was found that streamwise velocity fluctuations at the centre of the baths reached stationary values within five minutes, irrespective of bath size, which supports the idea that the flow was largely controlled by particle motion rather than surface effects. The flows also were stationary within experimental uncertainties once the initial transient period had ended.

Ideally, mean velocities in the bath would be small, however, lower particle number fluxes near the walls induced a large-scale circulation within the bath. Thus, the results summarized in table 1 indicate that $\bar{u}/(\overline{u'^2})^{\frac{1}{2}}$ was *c.* 0.5 for the lowest loadings of the 0.5 and 1.0 mm diameter particles, while this ratio varied in the range 0.7–1.0 for the other test conditions. Cross-stream mean velocities, however, were smaller, with $\bar{v}/(\overline{u'^2})^{\frac{1}{2}}$ less than 0.5 for all test conditions. The mean liquid velocities in the bath were small in comparison to particle terminal velocities so that their presence did not affect particle dynamics appreciably. Furthermore, since the flow was homogeneous and stationary, the mean motion did not influence velocity fluctuations, cross-correlations of velocity fluctuations and spatial correlations. However, the presence of a mean velocity did influence the temporal spectra; therefore, a correction was applied to these measurements which will be discussed later.

Ideally, the Reynolds stresses, $\overline{u'v'}$, should be zero for a homogeneous turbulent flow. This property was measured for the 0.5 mm diameter particles, for dissipation rates in the range 53.2–134.1 mm^2/s^3, finding $\overline{u'v'}/\bar{u}'^2 < 6\%$. Experimental uncertainties were large (55%) for the Reynolds stress measurements due to their small magnitude; therefore, these values are essentially zero within experimental uncertainties.

4.2. *Velocity fluctuations*

Measured velocity fluctuations in the streamwise and cross-stream directions are plotted as a function of dissipation for all three particle sizes in figure 5. Results for many test conditions other than those summarized in table 1 are plotted so that trends with dissipation and particle size can be seen more clearly.

The measurements for each component of velocity fluctuations illustrated in figure 5 vary solely as a function of dissipation within experimental uncertainties. Thus, effects of variations of particle number flux or spacing are represented by the dissipation through (4) while particle size is a secondary factor over the present test range. The cross-stream velocity fluctuations at the two highest loadings for the 0.5 mm diameter particles are a possible exception to this trend. However, these conditions had the highest particle number densities that were considered and are felt to be less reliable than the rest due to poorer signal-to-noise ratios. In accord with the general expectations from the theory, the ratio of streamwise to cross-stream velocity fluctuations is a constant, roughly 2, independent of test conditions, while both components of the velocity fluctuations are proportional to $\epsilon^{\frac{1}{2}}$. The larger streamwise velocity fluctuations are understandable since liquid motion primarily is caused by particles moving in the streamwise direction. This high level of anisotropy also suggests relatively strong effects of particle wakes; otherwise, the flow would be more isotropic, analogous to conditions somewhat downstream of a turbulence-generating grid.

Predicted velocity fluctuations were found by roughly matching predicted streamwise velocity fluctuations, allowing for both mean and turbulent wake properties, with the measurements. This involved terminating the integration of

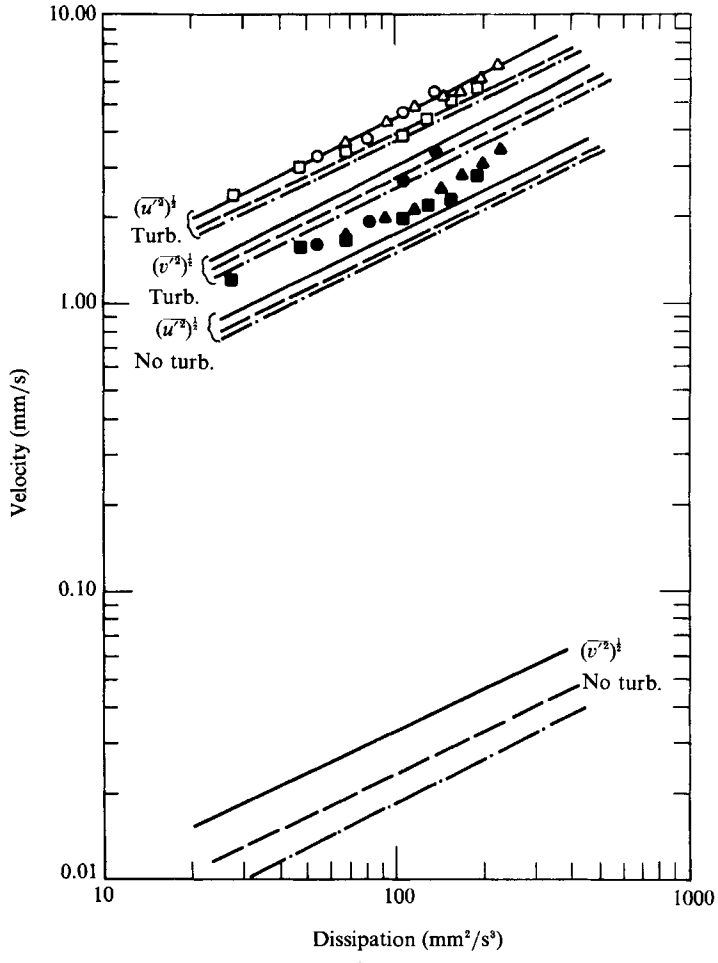

FIGURE 5. Liquid velocity fluctuations: ○, ●, measurements, ——, predictions for $d_p = 0.5$ mm; □, ■, measurements, – – –, predictions for $d_p = 1.0$ mm; ▽, ▼, measurements, —·—, predictions for $d_p = 2.0$ mm. Open and closed symbols denote streamwise and cross-stream velocity fluctuations, respectively.

wake properties at $x/d_p = U_\infty T_\infty/d_p = 175$. This choice also seems reasonable on a physical basis. The mean velocity defect on the axis at this location is on the order of 1% of the terminal velocity, and comparable to the streamwise velocity fluctuations, so that it is likely that the coherence of wake properties would be lost in the background turbulence at larger distances. Thus, in a sense, this location is analogous to the location where the flow becomes nearly isotropic downstream of a turbulence-generating grid. Notably, although the fundamental limit problem remains, the sensitivity of predicted velocity fluctuations to the value of T_∞ is relatively weak, e.g. ignoring the contribution of the potential flow region, velocity functions are proportional to $T_\infty^{\frac{1}{6}}$, see (25), (26) and (30).

With this selection of T_∞ predicted velocity fluctuations, including both mean and fluctuating wake properties, become

$$\overline{u'^2}U_\infty/(\epsilon d_p) = 46.72(\theta/d_p)^{\frac{2}{3}}, \tag{32}$$

$$\overline{v'^2}U_\infty/(\epsilon d_p) = 21.49(\theta/d_p)^{\frac{2}{3}}. \tag{33}$$

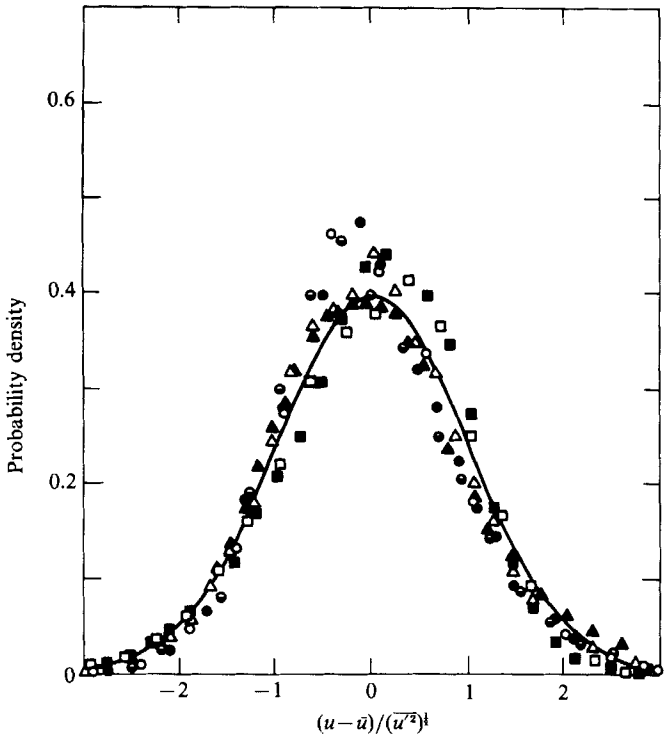

FIGURE 6. Probability density functions of streamwise liquid velocity fluctuations: □, ■, d_p = 0.5 mm, ϵ = 53.2, 106.3 mm^2/s^3; ○, ◒, ●, d_p = 1.0 mm, ϵ = 27.3, 68.2, 155.8 mm^2/s^3; ▽, ▼, d_p = 2.0 mm, ϵ = 67.1, 193.5 mm^2/s^3; ——, prediction.

A useful alternative formulation can be obtained by introducing expressions for U_∞ and θ in (32) and (33). As noted earlier, mean particle velocities in the bath were essentially the same as terminal velocities in a still environment, yielding

$$U_\infty = (4gd_p(\rho_p/\rho - 1)/(3C_D))^{\frac{1}{2}}. \tag{34}$$

Then substituting (20) for θ and (34) for U_∞ into (32) and (33) yields

$$\frac{\overline{u'^2}}{\epsilon}\left[\frac{g}{d_p}\left(\frac{\rho_p}{\rho}-1\right)\right]^{\frac{1}{2}} = 20.24C_D^{\frac{5}{6}}, \tag{35}$$

$$\frac{\overline{v'^2}}{\epsilon}\left[\frac{g}{d_p}\left(\frac{\rho_p}{\rho}-1\right)\right]^{\frac{1}{2}} = 9.31C_D^{\frac{5}{6}}. \tag{36}$$

Equations (35) and (36) show that velocity fluctuations vary with particle diameter as $d_p^{\frac{1}{4}}C_D^{\frac{5}{12}}$: this yields roughly a 20% reduction of the velocity fluctuations for a particular value of ϵ as d_p goes from 0.5 to 2.0 mm.

Equations (35) and (36), along with their counterparts when effects of wake turbulence are ignored using the same T_∞, are plotted in figure 5. Predictions with and without wake turbulence were considered since present wake Reynolds numbers were low in comparison to those considered by Uberoi & Freymuth (1970) so that wake turbulence may not be as well-developed for present test conditions. The predictions illustrated in figure 5 suggest that this is not the case. In particular, predictions of cross-stream velocity fluctuations are much smaller than measured cross-stream velocity fluctuations when the contributions of wake turbulence are ignored. This is

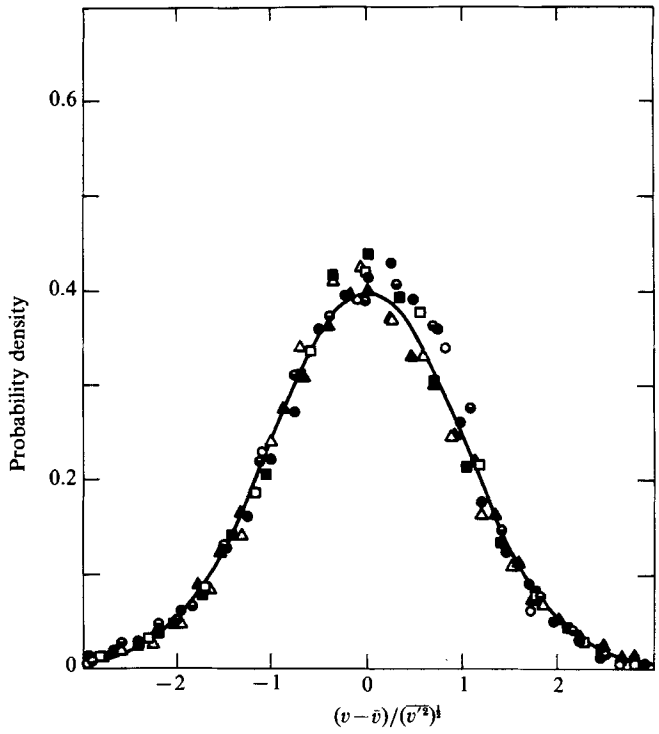

FIGURE 7. Probability density functions of cross-stream liquid velocity fluctuations: see caption of figure 6 for symbols.

not an effect of the selection of T_∞ since the prediction of $\overline{v'^2}$ from (26) does not diverge as $T_\infty \to \infty$ and yields essentially the same results as $U_\infty T_\infty / d_p = 175$. Rather, cross-stream mean velocities are much smaller than streamwise mean velocities in wakes, as well as velocity fluctuations in turbulent wakes. On the other hand, the ratio of streamwise-to-cross-stream velocity fluctuations from (35) and (36) is 1.47, which is somewhat less than the value of roughly 2 of the measurements. This might be explained by turbulence levels in particle wakes being lower than the levels found by Uberoi & Freymuth (1970) due to the much lower Reynolds numbers of the present particle wakes. Based on these observations, it seems probable that both mean and turbulent wake properties contribute to the turbulence field.

Estimates of velocity fluctuations from (35) and (36) vary with particle diameter as noted earlier. However, this variation is comparable to experimental uncertainties and a similar trend is not seen in the measurements illustrated in figure 5. The degree of development of the turbulence in the wake may also be a factor in the reduced sensitivity of the measurements to particle diameter. In particular, predictions indicate lower levels of turbulent fluctuations with increased particle diameter while larger particles have higher wake Reynolds numbers which should tend to increase wake turbulence levels; therefore, these two effects tend to counteract one another. Additional measurements of turbulent properties in the present Reynolds number range would be helpful in resolving this issue.

The p.d.f.s of streamwise and cross-stream velocity fluctuations are plotted as a function of normalized variables in figures 6 and 7. Within experimental uncertainties, measurements are generally independent of particle size and loading. Predictions based on a Gaussian p.d.f., which is the form expected from the theory,

are also illustrated on each plot. This distribution is in good agreement with the measurements but this is not a strong test of predictions since velocity fluctuations in homogeneous turbulence generally exhibit Gaussian p.d.f.s.

4.3. *Temporal spectra*

Measured normalized temporal power spectral densities of streamwise and cross-stream velocity fluctuations are plotted as a function of normalized frequency in figures 8 and 9. The integral timescales of streamwise and cross-stream velocity fluctuations, T_u and T_v, used in the normalizations, will be taken up later. The measurements are limited to the lowest loadings of all three particle diameters for the streamwise spectra but just the 0.5 mm diameter particle for the cross-stream spectra. These limitations were necessary in order to select conditions that were not unduly influenced by effects of mean velocities that were mentioned earlier.

Two experimental problems must be considered before discussing the measured temporal spectra: the effect of mean velocities and the effect of step noise. Mean streamwise velocities are generally much larger than mean cross-stream velocities for the conditions plotted in figures 8 and 9; therefore, effects of the latter will be ignored. When there is a mean streamwise velocity, the streamwise temporal correlation measured at a fixed point is $\overline{u'(x-\bar{u}t, y, z, t)\, u'(x-\bar{u}(t+\tau), y, z, t+\tau)}$ which is actually a two-point, two-time correlation rather than $\overline{u'(x, y, z, t)\, u'(x, y, z, t+\tau)}$ which is the temporal correlation that is being sought (Hinze 1975). In order to correct for the effect of the mean velocity, it was assumed that the combined correlation could be decomposed into a product of temporal and spatial correlations:

$$\overline{u'(x-\bar{u}t, y, z, t)\, u'(x-\bar{u}(t+\tau), y, z, t+\tau)} = \overline{u'(x-\bar{u}t, y, z, t)\, u'(x-\bar{u}(t+\tau), y, z, t)}\;\overline{u'(x, y, z, t)\, u'(x, y, z, t+\tau)}/\bar{u}'^2. \quad (37)$$

Equation (37) is not rigorously accurate, however, it is a reasonable approximation for a homogeneous turbulent field. Since the measured spatial correlations in the streamwise direction were unaffected by the mean velocity, $\overline{u'(x-\bar{u}t, y, z, t)\, u'(x-\bar{u}(t+\tau), y, z, t)}$ is known from present measurements so that the temporal correlation $\overline{u'(x, y, z, t)\, u'(x, y, z, t+\tau)}$ can be calculated from (37). Taking the Fourier transform of this correlation then yields the spectra illustrated in figure 8. The correction for mean velocities was negligible for the lowest loading of the 0.5 mm diameter particles and was relatively small (less than 10%) for the lowest loadings of the other two particle sizes; therefore, only measurements for these conditions are plotted in figure 8.

In order to apply a similar correction for the presence of mean velocities to the temporal correlation of cross-stream velocity fluctuations, the spatial correlation $\overline{v'(x-\bar{u}t, y, z, t)\, v'(x-\bar{u}(t+\tau), y, z, t)}$ must be known; unfortunately, this spatial correlation was not measured. However, since the mean velocity correction was small for the temporal correlation of streamwise velocity fluctuations for the lowest loading with the 0.5 mm diameter particles, it was assumed that the correction would be small for the temporal correlation of the cross-stream velocity fluctuations at this condition as well – which are the only measurements plotted in figure 9.

The second problem is that Fourier transformation of the analogue signal of the LV burst processor introduced 'step-noise' caused by the sample-and-hold signals of the processor. Adrian & Yao (1987) have shown that effects of step-noise are observed at frequencies roughly one-tenth of the frequency corresponding to the mean data rate. The characteristics of step-noise are the appearance of a noise band having a constant spectral amplitude followed by a second-order low-pass filter effect

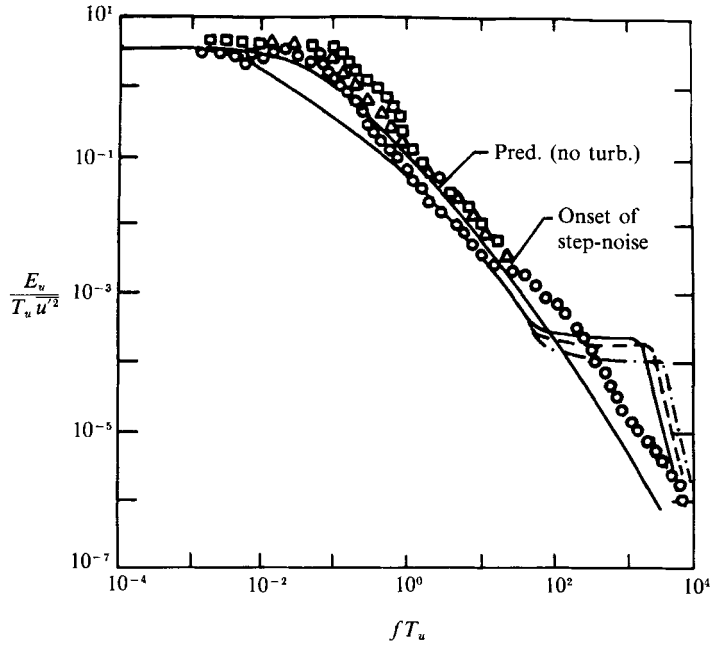

FIGURE 8. Temporal spectral densities of streamwise liquid velocity fluctuations: ○, $d_p = 0.5$ mm, $\epsilon = 53.2$ mm^2/s^3, ——, prediction; □, $d_p = 1.0$ mm, $\epsilon = 27.3$ mm^2/s^3, – – –, prediction; △, $d_p = 2.0$ mm, $\epsilon = 67.1$ mm^2/s^3, —·—, prediction.

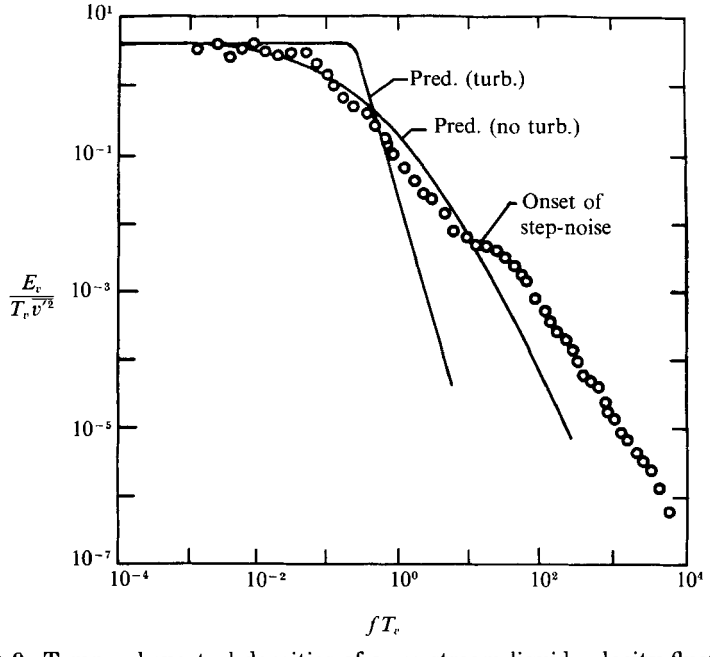

FIGURE 9. Temporal spectral densities of cross-stream liquid velocity fluctuations: ○, $d_p = 0.5$ mm, $\epsilon = 53.2$ mm^2/s^3, ——, prediction.

at a slightly higher frequency, i.e. a subsequent decay of the spectra according to f^{-2}. This yields a slight flat spot in the spectra followed by a region where the spectra decrease according to f^{-2} which is noted in figures 8 and 9 for the measurements with the 0.5 mm diameter particles.

The onset of step-noise for present measurements with the 0.5 mm diameter particles corresponds to the estimates of Adrian & Yao (1987). For example, the streamwise spectrum in figure 8 exhibits a change in slope (denoted step-noise in the figure) at $fT_u \sim 10$ which roughly corresponds to one-tenth of the mean data rate (2000 Hz). The onset of step-noise appears at a slightly lower frequency for the cross-stream spectrum in figure 9 which is consistent with the slightly lower data rate of these measurements. Naturally, the portions of the spectra beyond the onset of step-noise are not representative of flow properties and should be ignored: the region is only illustrated in figures 8 and 9 in order to establish that this portion is an artifact of step-noise and not some property of the flow since the predictions also suggested the presence of steps in the streamwise temporal spectra at high frequencies.

A correction for step-noise was made at the same time as the mean velocity corrections for the measurements with the 1.0 and 2.0 mm diameter particles; therefore, the step-noise region is not illustrated for these measurements in figure 8. The corrections involved subtracting the step-noise from the spectrum, taking the Fourier transform of the result to obtain the combined temporal and spatial correlation, applying the mean velocity correction to this correlation, and finally taking the Fourier transform of this correlation to obtain the results illustrated in figure 8.

The differences between the measured temporal spectra of streamwise velocity fluctuations for the three particle diameters illustrated in figure 8 are not significant in comparison to experimental uncertainties. This is consistent with the measurements of streamwise velocity fluctuations, illustrated in figure 4, where it was found that effects of particle diameter are not very important. In addition to differences of particle diameters, the measurements illustrated in figure 8 also have different rates of dissipation; however, it was a general conclusion of the theory that temporal correlations should be independent of the rate of dissipation. Based on these findings, the small effect of particle diameter on the spectra illustrated in figure 8 is quite reasonable.

Perhaps the most surprising feature of the spectra of streamwise velocity fluctuations illustrated in figure 8 is the large range of frequencies in the spectra, even though wake Reynolds numbers are relatively low; and the significant levels of signal energy at very low frequencies, even though the flow field is produced by small high-velocity particles having relatively large interparticle spacings. In fact, based on the theoretical estimates, the measured spectra would have extended over a much larger frequency range if the limitations of step-noise could have been avoided. The reason for this large range of frequencies, as well as the presence of appreciable signal energy at the low frequencies, is that the flow includes contributions from both the mean and turbulent velocity fields of the particle wakes while the mean velocities enhance signal energies at low frequencies. Such behaviour is not normally observed in turbulent flows generated by other mechanisms; however, the contributions of mean velocities cannot be separated from the contributions of turbulence in the particle wakes for present flows since particle arrivals are random.

Since predicted normalized temporal spectra were not sensitive to the selection of T_∞, a large value was chosen, $x/d_p = U_\infty T_\infty/d_p = 25000$, to cover the complete normalized frequency range of figures 8 and 9. The effect of this selection on

predictions of integral scales will be taken up later. Predictions of streamwise temporal spectra considering and ignoring wake turbulence in figure 8 were independent of dissipation rates while predictions ignoring wake turbulence were independent of particle diameter as well. However, predictions considering wake turbulence exhibit somewhat different shapes at high frequencies, reflecting effects of different wake Reynolds numbers for the different sized particles.

Similar to the measurements, predictions of streamwise temporal spectra, both considering and ignoring wake turbulence, exhibit significant signal energy at low frequencies in figure 8: this supports the idea that the low-frequency region is caused by mean velocities in the particle wakes since both predictions include this contribution. Unfortunately, the portion of the spectra that involves the contribution of wake turbulence could not be observed directly due to effects of step-noise. The agreement between predicted and measured temporal spectra of streamwise velocity fluctuations is within the scatter of the data in the region that is not affected by step noise, although quantitative agreement is somewhat better when wake turbulence is ignored. This suggests that the turbulence of the particle wakes may not be developed to the extent observed by Uberoi & Freymuth (1970), which would not be surprising since present wake Reynolds numbers are much lower.

Measurements of the temporal spectra of cross-stream velocity fluctuations, illustrated in figure 9, exhibit trends similar to the temporal spectra of streamwise velocity fluctuations: there is significant signal energy at low frequencies and probably a large range of frequencies in the spectra, if step-noise had not intruded, since both mean and turbulent properties of particle wakes contribute to the spectra. Due to the small magnitude of mean radial velocities in comparison to radial velocity fluctuations in wakes, however, the turbulence contributions to the cross-stream spectra are two orders of magnitude higher than the mean velocity contributions; therefore, the cross-stream spectra provide a more sensitive indication of wake turbulence effects than the streamwise turbulence spectra – analogous to the relative effect of wake turbulence on cross-stream and streamwise velocity fluctuations that was discussed earlier. Thus, the shapes of the predicted spectra with and without wake turbulence differ to a greater extent for the cross-stream velocity fluctuations. The measurements in the step-noise-free portion of the spectrum lie between the two predictions, which suggests a lower degree of development of wake turbulence than observed by Uberoi & Freymuth (1970) at higher wake Reynolds numbers. While this is plausible, additional measurements of the properties of turbulent wakes behind spheres at moderate Reynolds numbers would greatly help to resolve the properties of homogeneous particle-laden flows.

4.4. *Spatial correlations*

The measured spatial correlations of streamwise velocity fluctuations in the cross-stream direction are illustrated in figure 10. Measurements at various particle loadings for the three particle diameters are plotted as a function of cross-stream distance normalized by the cross-stream integral lengthscale, L_{uy}. Consideration of the cross-stream integral lengthscales themselves will be taken up later. These measurements were repeated for both positive and negative separation distances to check the symmetry of the correlations. These results are not illustrated to avoid crowding of the figure, however, they showed that the correlations were symmetric within experimental uncertainties.

The spatial correlation measurements for various loadings and particle sizes are essentially the same. This is consistent with the general conclusion of the theory that

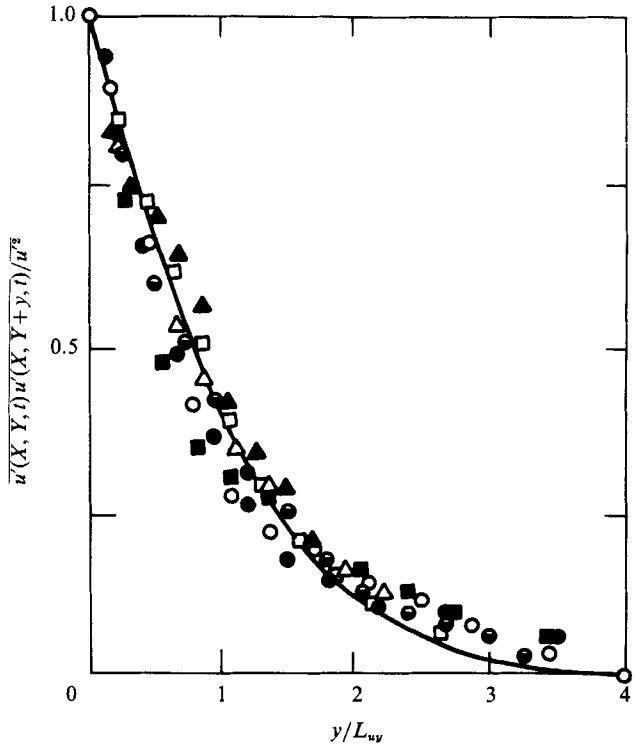

FIGURE 10. Spatial correlations of streamwise liquid velocity fluctuations in the cross-stream direction: □, ■, $d_p = 0.5$ mm, $\epsilon = 53.2$, 106.3 mm^2/s^3; ○, ◒, ●, $d_p = 1.0$ mm, $\epsilon = 27.3$, 68.2, 155.8 mm^2/s^3; △, ▲, $d_p = 2.0$ mm, $\epsilon = 67.1$, 193.5 mm^2/s^3, ——; prediction.

correlation coefficients should be independent of the rate of dissipation, and the earlier finding that velocity fluctuations are relatively independent of particle size. The measurements exhibit an exponential-like decay of the correlation with increasing separation distances. This observation is influenced to some extent by experimental problems since effects of step-noise precluded resolving the smallest scales of the flow that would be expected to influence the curvature of the correlation at the smallest separation distances (Hinze 1975).

Predictions of spatial correlations used the same T_∞ as the temporal spectra. The prediction of the spatial correlation of streamwise velocity fluctuations in the cross-stream direction, illustrated in figure 10, had to be limited to consideration of only mean properties in the particle wakes. To include effects of wake turbulence in these predictions would require measurements of lateral correlations in turbulent wakes and no such measurements have been reported. However, since the measurements emphasize the large-scale features of the flow, which are also emphasized by predictions using only mean wake properties, comparing this prediction with measurements is reasonable. In agreement with the measurements, the prediction indicates that the correlation should be independent of particle loading and size. The quantitative agreement between the predictions and measurements is reasonably good for small separation distances, however, the predictions decay more rapidly than the measurements at large separation distances. Reasons for this behaviour will be considered when integral scales are discussed.

The measured spatial correlations of streamwise velocity fluctuations in the streamwise direction are illustrated in figure 11. Measurements for various particle

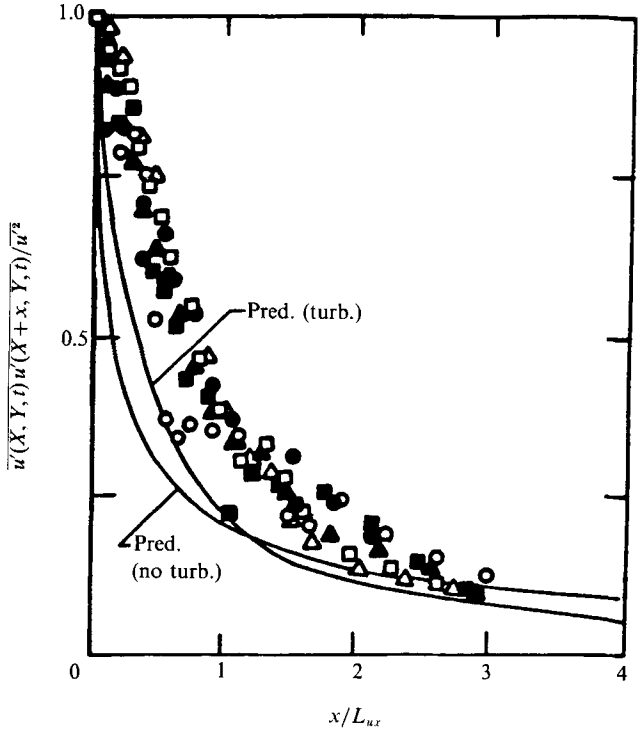

FIGURE 11. Spatial correlations of streamwise liquid velocity fluctuations in the streamwise direction: see caption of figure 10 for symbols.

diameters and loadings are plotted as a function of streamwise separation distance normalized by the streamwise integral lengthscale, L_{ux}. The data scatter of the correlations for the streamwise direction is somewhat greater than the correlations for the cross-stream direction. However, within experimental uncertainties, the correlation is independent of particle loading and size. The reasons for this behaviour are the same as for the lateral correlations.

For correlations in the streamwise direction, spatial correlations needed to compute the contribution of wake turbulence are available, therefore, predictions both considering and ignoring the contribution of wake turbulence are illustrated in figure 11. In agreement with the measurements, both predictions are essentially independent of particle size and loading over the present test range. When wake turbulence is ignored, the correlation decreases quite rapidly at small separation distances since the flow is dominated by relatively large lengthscales associated with the mean velocity profiles of the wake. Considering wake turbulence places a greater degree of the signal energy at the smaller lengthscales associated with the turbulence: this reduces the rate of decline of the correlation at small separation distances and yields a correspondingly more rapid decrease of the correlation at large separation distances. However, differences between the two predictions are comparable to experimental uncertainties and neither is in particularly good agreement with measurements: the predictions overestimate the initial rate of decrease and exhibit a longer tail than the measurements.

d_p (mm)	0.5	1.0	2.0
T_u (s):			
Measured[a]	6	7	7
Predicted (turb.)[b]	10 (21)	10 (21)	12 (21)
Predicted (no turb.)[c]	130 (225)	130 (225)	130 (225)
T_v (s):			
Measured[a]	4	—	—
Predicted (turb.)[b]	0.001	0.001	0.001
Predicted (no turb.)[c]	0.17	0.17	0.17
L_{uy} (mm):			
Measured[d]	17 (2)	15 (2)	21 (3)
Predicted (turb.)[b]	—	—	—
Predicted (no turb.)[c]	2	4	7
L_{ux} (mm):			
Measured[d]	59 (2)	59 (6)	57 (2)
Predicted (turb.)[b]	70 (710)	140 (1900)	280 (5600)
Predicted (no turb.)[c]	850 (9200)	1700 (23700)	2550 (59800)

[a] Measured for lowest particle loading only.
[b] Predicted assuming $x/d_p = U_\infty T_\infty/d_p = 175$. Numbers in parentheses are for $x/d_p = 25000$.
[c] Predicted assuming $x/d_p = U_\infty T_\infty/d_p = 2730$. Numbers in parentheses are for $x/d_p = 25000$.
[d] Average value for loading range of table 1. Standard deviation is in parentheses.

TABLE 2. Measured and predicted integral timescales and lengthscales

4.5. *Integral timescales and lengthscales*

Measured and predicted integral time and lengthscales are summarized in table 2. Integral lengthscales were measured for the full range of particle loadings, however, integral timescales were only measured for the lowest particle loadings due to uncertainties in correcting for mean velocities noted earlier. The measured integral scales are relatively independent of test conditions. This is remarkable since most experimental variables that might be expected to influence integral scales were varied over a wide range: particle diameters from 0.5 to 2.0 mm, mean particle spacings from 8 to 62 mm, and rates of dissipation from 27 to 194 $mm^2 s^3$. The small effect of dissipation on integral scales is expected from the theory, which implies small effects of particle number flux and spacing through (3) and (4) as well. However, the small effects of particle diameter and spacing is surprising, although effects of these properties also were small for velocity fluctuations, p.d.f.s of velocities, and spatial and temporal correlations.

The ratio between measured streamwise and cross-stream temporal integral scales in table 2 is roughly 1.5, however, the available data base for this ratio is relatively limited. The ratio between streamwise and cross-stream spatial integral scales is roughly 3, which reflects the high level of anisotropy of the present flows. This degree of anisotropy also supports the idea that wake-like properties, rather than loss of wake coherence and approach to isotropic turbulence, are dominant features of the present flows.

Predicted integral scales, considering and ignoring wake turbulence, also are summarized in table 2. T_∞ was chosen to match measured streamwise velocity fluctuations for baseline predictions: taking $x/d_p = U_\infty T_\infty/d_p = 175$ and 2730 when wake turbulence was considered and ignored. The sensitivity of predicted integral scales to variations in T_∞ is also indicated in table 2 by including results for $x/d_p =$

$U_\infty T_\infty/d_p = 25000$ which was the value used for temporal spectra and spatial correlations in figures 8–11.

Predicted integral scales in table 2 are properly independent of the rate of dissipation but are generally unsatisfactory otherwise. A possible exception is T_u considering turbulence, where predicted and measured magnitudes and trends were similar. For the rest, T_v is vastly underestimated by predictions, particularly when turbulence is considered; predictions of T_u and L_{ux} are vastly overestimated when turbulence is ignored; and predicted spatial integral scales exhibit variations with particle diameter that are not supported by the measurements. Furthermore, the convergence problem that required an *ad hoc* selection of T_∞ has a significant impact on predictions of L_{ux} owing to its sensitivity to this choice. Finally, no compromise selection of T_∞ could be found that provides good predictions of both velocity fluctuations and integral scales.

4.6. *Discussion*

In spite of numerous simplifications, the theory was helpful for explaining many features of the measurements, and the predictions were generally reasonable. However, the convergence problem when particle wakes are evaluated, and the relatively poor predictions of integral scales and streamwise spatial correlations, are disconcerting. Two phenomena that may be responsible for these difficulties are discussed in the following: disturbances of wakes due to turbulent dispersion of particles, and the structure of particle wakes in the present turbulent environment.

Recall that predictions were based on particles settling along vertical lines, i.e. effects of turbulent dispersion of particles were ignored. For present experimental conditions, however, turbulent dispersion was significant and cross-stream particle and liquid velocity fluctuations were comparable (Parthasarathy & Faeth 1990). Thus, particle wakes were actually deposited along sinuous paths – affecting the apparent width of the wakes, and augmenting cross-stream velocity fluctuations by placing a component of the mean velocity along the wake axis into a horizontal plane. Since wakes grow relatively slowly in the radial direction, and have small mean radial velocities, these effects can be significant for homogeneous particle-laden flows.

Dye tracks released into the wakes of individual particles were photographed in order to help quantify potential effects of turbulent dispersion of particles. Considering only fresh wakes, with the particle still in view, showed that the projected cross-stream displacements of particles were comparable to characteristic wake radii (based on the mean streamwise velocity being 1–5% of the mean streamwise velocity at the axis), e.g. 2–6 mm for $x/d_p = 175$. This behaviour is consistent with cross-stream liquid and particle velocity fluctuations being comparable. Rough calculations showed that this effect was sufficient to increase predictions of L_{uy} to the range of the measurements and reduce its sensitivity to particle diameter; thus, the effect is significant. Additionally, projected particle tracks were oriented up to 10° from the vertical direction which causes momentum along the wake axis to be deposited into the cross-stream direction: this would tend to reduce potential effects of wake turbulence inferred earlier and modify predictions of cross-stream scales as well. Thus, the nonlinear interaction between turbulent dispersion of particles in the turbulent field that they create must be considered when defining the particle flow field for predictions using the present approach.

Another nonlinear interaction is the effect of the turbulent field generated by the particles on the properties of their wakes. Present predictions were based on the properties of wakes for rigidly-mounted spheres in a non-turbulent environment.

Turbulent dispersion of particles – and the deflection, distortion and improved mixing of wakes in a turbulent environment – are likely to modify behaviour from wakes in a non-turbulent environment. In particular, wakes in a turbulent environment should mix more quickly and observe different scaling rules than wakes in non-turbulent environments (Tennekes & Lumley 1972). For example, similarity was assumed to obtain the turbulent wake properties of (21)–(23) with specific results requiring a turbulent viscosity that is constant over the wake cross-section and decreases with increasing streamwise distance. Such scaling is unlikely to be relevant for wakes having modest Reynolds numbers in a turbulent environment, and proper scaling might resolve the convergence problem directly. Finally, as mentioned earlier, little is known about the turbulent structure of wakes at the modest Reynolds numbers of present tests, which also affects predictions.

Clearly, further progress concerning turbulence modulation in homogeneous dilute particle-laden flows will require a better understanding of particle wake properties. This includes the structure of turbulent wakes at moderate Reynolds numbers, the structure of wakes in turbulent environments, and the structure of wakes of freely-moving particles undergoing turbulent dispersion.

5. Conclusions

The present investigation considered the continuous-phase properties of homogeneous dilute particle-laden flows. The specific configuration involved nearly monodisperse glass spheres (particle diameters of 0.5, 1.0 and 2.0 mm with corresponding Reynolds numbers of 38, 156 and 545) falling in a water bath. Experimental conditions were as follows: turbulence number fluxes of 1.1–110.8 kpart m^2/s, mean particle spacings of 8.2–61.8 mm, rates of dissipation of 27.3–193.5 mm^2/s^3 and particle volume fractions less than 0.01%. The major observations and conclusions of the study are as follows:

(i) Velocity fluctuations could be correlated solely as a function of the rate of dissipation of particle energy in the liquid.

(ii) Streamwise velocity fluctuations were roughly twice cross-stream velocity fluctuations for all test conditions, suggesting a significant influence of the wakes behind individual particles on the properties of the flow.

(iii) Normalized temporal spectra, spatial correlation coefficients, and temporal and spatial integral scales were relatively independent of both particle size and the rate of dissipation of particle energy in the liquid.

(iv) Temporal spectra indicated a large range of frequencies even though particle and wake Reynolds numbers were relatively small, since both mean and fluctuating properties of the particle wakes contributed to the spectra because particle arrivals were random.

(v) An analysis based on linear superposition of undistorted particle wakes in a non-turbulent environment predicted many properties of the flow reasonably well. However, it yielded poor estimates of integral scales and streamwise spatial correlations. These deficiencies are attributed largely to effects of turbulent dispersion of the particles and effects of the ambient turbulence field on the structure of the wakes.

(vi) Linear superposition of particle wakes in the analysis presented convergence problems, similar to convergence problems encountered during analysis of sedimentation processes. This was resolved by assuming that only the near-field region of the wakes, $x/d_p = T_\infty U_\infty/d_p < 175$, would maintain sufficient coherence to

contribute to flow properties as a wake – a choice that matched predictions and measurements of streamwise velocity fluctuations. However, a more rational resolution of the convergence problems should be sought.

(vii) Particle-laden flows typically involve turbulent dispersion of particles and particle Reynolds numbers less than 1000 within a turbulent environment: more information is needed concerning the mean and turbulent structure of wakes under these conditions in order to address the difficulties of the present analysis in a rational manner.

The authors wish to thank L. P. Bernal and W. W. Willmarth for helpful discussions during the course of the study. The work was supported by the Air Force Office of Scientific Research, Grant no. AFOSR-85-0244, under the technical management of J. M. Tishkoff. The US Government is authorized to reproduce and distribute copies of this paper for Governmental purposes notwithstanding any copyright notation thereon.

REFERENCES

ADRIAN, R. J. & YAO, C. S. 1987 Power spectra of fluid velocities measured by laser Doppler velocimetry. *Exps Fluids* **5**, 17–28.

AL TAWEEL, A. M. & LANDAU, J. 1977 Turbulence modulation in two-phase jets. *Intl J. Multiphase Flow* **3**, 341–351.

BATCHELOR, G. K. 1972 Sedimentation in a dilute dispersion of spheres. *J. Fluid Mech.* **52**, 245–268.

BATCHELOR, G. K. 1973 *An Introduction to Fluid Dynamics*, pp. 450–455. Cambridge University Press.

FAETH, G. M. 1987 Mixing, transport and combustion in sprays. *Prog. Energy Combust. Sci.* **13**, 293–345.

HINO, M. 1968 Turbulent flow with suspended particles. *ASCE J. Hydrol.* **4**, 161–185.

HINZE, J. O. 1972 Turbulent fluid and particle interaction. *Prog. Heat Mass Transfer* **6**, 433–452.

HINZE, J. O. 1975 *Turbulence*. McGraw-Hill.

KADA, E. J. & HANRATTY, T. J. 1960 Effects of solids on turbulence in a fluid. *AIChE J.* **6**, 624–630.

KUCHANOV, S. I. & LEVICH, V. G. 1967 Motion of particles suspended in turbulent flow. *Sov. Phys. Dokl.* **12**, 546–548.

LANCE, M. & BATAILLE, J. 1982 Turbulence in the liquid phase of a bubbly air–water flow. *Advances in Two-Phase Flow and Heat Transfer*, vol. 1, pp. 403–427, Martinus Nijhof.

LANCE, M., MARIE, J. L. & BATAILLE, J. 1985 Homogeneous turbulence in bubbly flows. Publication *FEP*-29, ASME, 117–124.

LANCE, M., MARIE, J. L., CHARNAY, G. & BATAILLE, J. 1980 Turbulence structure of a cocurrent air–water bubbly flow. *NUREG/CP*-0014. Nuclear Regulatory Commission, Washington, vol. 2, pp. 403–427.

MICHAELIDES, E. E. & STOCK, 1989 *Turbulence modification in dispersed multiphase flows*, *FED*-vol. 80, ASME, NY.

MODARRESS, D., TAN, H. & ELGHOBASHI, S. 1984 Two-component LDA measurements in a two-phase turbulent jet. *AIAA J.* **22**, 624–630.

OWEN, P. R. 1964 Saltation of uniform grains in air. *J. Fluid Mech.* **20**, 225–242.

OWEN, P. R. 1969 Pneumatic transport. *J. Fluid Mech.* **39**, 407–432.

PARTHASARATHY, R. N. 1989 Homogeneous dilute turbulent particle-laden water flow. PhD thesis, The University of Michigan.

PARTHASARATHY, R. N. & FAETH, G. M. 1987 Structure of particle-laden turbulent water jets in still water. *Intl J. Multiphase Flow* **13**, 699–716.

PARTHASARATHY, R. N. & FAETH, G. M. 1990 Turbulent dispersion of particles in self-generated homogeneous turbulence. *J. Fluid Mech.* **220**, 515–537.

PUTNAM, A. 1961 Integrable form of droplet drag coefficient. *ARS J.* **31**, 1467–1468.

RICE, S. O. 1954 Mathematical analysis of random noise. *Noise and Stochastic Processes*, pp. 133–194. Dover.

SHUEN, J.-S., SOLOMON, A. S. P., ZHANG, Q.-F. & FAETH, G. M. 1985 Structure of particle-laden jets: measurements and predictions. *AIAA J.* **21**, 1480–1483.

SOLOMON, A. S. P., SHUEN, J.-S., ZHANG, Q.-F. & FAETH, G. M. 1985 Structure of nonevaporating sprays: II. drop and turbulence properties. *AIAA J.* **23**, 1724–1730.

SUN, T.-Y. & FAETH, G. M. 1986 Structure of turbulent bubbly jets. II. phase property profiles. *Intl J. Multiphase Flow* **12**, 115–124.

TENNEKES, H. & LUMLEY, J. L. 1972 *A First Course in Turbulence*, pp. 113–124, MIT Press.

UBEROI, M. S. & FREYMUTH, P. 1970 Turbulent energy balance and spectra of the axisymmetric wake. *Phys. Fluids* **13**, 2205–2210.